Microporous and Mesoporous Materials 305 (2020) 110391

Contents lists available at ScienceDirect

Microporous and Mesoporous Materials

journal homepage: http://www.elsevier.com/locate/micromeso

Selectively capturing carbon dioxide from mixed gas streams using a new microporous organic copolymer

Ahmed M. Alloush [a,b], Mahmoud M. Abdelnaby [a,c], Kyle E. Cordova [d], Naef A.A. Qasem [e], Bassem A. Al-Maythalony [b], Almaz Jalilov [a], Youcef Mankour [f], Othman Charles S. Al Hamouz [a,*]

[a] Department of Chemistry, King Fahd University of Petroleum and Minerals (KFUPM), Dhahran, 31261, Saudi Arabia
[b] King Abdulaziz City for Science and Technology – Technology Innovation Center on Carbon Capture and Sequestration (KACST-TIC on CCS), KFUPM, Dhahran, 31261, Saudi Arabia
[c] Center for Research Excellence in Nanotechnology (CENT), KFUPM, Dhahran, 31261, Saudi Arabia
[d] Materials Discovery Research Unit, Reticular Foundry, Royal Scientific Society, Amman, 11941, Jordan
[e] Department of Aerospace Engineering, King Fahd University of Petroleum & Minerals, Dhahran, 31261, Saudi Arabia
[f] Process & Control Systems Department, Upstream Engineering Division, Gas Processing Unit, Saudi Aramco, Dhahran, 31311, Saudi Arabia

ARTICLE INFO

Keywords:
Microporous organic polymers
Polymer chemistry
Carbon capture and sequestration
Gas separation

ABSTRACT

A novel crosslinked microporous polymer was synthesized via a modified acid-catalyzed Friedel-Crafts polycondensation reaction. By virtue of the rigid and polarizable monomers (aniline and pyrrole), the polymer, termed KFUPM-4, was proven permanently porous (Brunauer-Emmett-Teller surface area = 650 $m^2\ g^{-1}$) with a high CO_2 capacity (33 $cm^3\ g^{-1}$ at 760 Torr and 298 K) and selectivity (CO_2:CH_4 selectivity = 15:1 at 298 K). As a result of these properties, KFUPM-4 was subjected to breakthrough measurements, whereby the material's ability to selectively capture CO_2 under dynamic conditions from both dry and wet mixed gas streams was clearly demonstrated.

1. Introduction

Carbon dioxide emissions present a dramatic challenge to the environment as the continuous increase of its concentration in the atmosphere causes an elevation in the earth's temperature leading to significant climate change [1]. However, lowering carbon dioxide emissions from fossil fuel combustion remains a distant prospect as the demand for fossil fuel energy is still rising [2]. The development of new technologies whereby carbon dioxide is captured directly at point sources, prior to being released into the atmosphere, is a worthwhile pursuit that has attracted much interest over the past two decades [3,4]. One avenue that these new technologies are taking depend on solid adsorbent materials that possess special structural features to selectively exploit carbon dioxide's large quadrupole moment and polarizability [5]. Though, at this point, such CO_2-philic solid materials can be designed almost at will, rarely are the materials capable of retaining their CO_2-philic behaviors when other gases/vapors are present – most notably water vapor [6]. This is due to competitive adsorption between CO_2 and H_2O, which severely hinders the performance of porous, solid materials such as metal-organic frameworks (MOFs) [7,8], zeolites [9,10], and activated carbon [11,12].

Microporous organic polymers, with their unique structures and pore characteristics, are considered to be highly attractive for their potential application in various fields including, but not limited to, gas storage, catalysis, sensing, energy applications, conductivity and gas separation [13,14]. The feasibility and relative ease of design and synthesis using simple monomers has led to a class of materials that embody: (i) high surface area based on well-defined, rigid monomers; (ii) exceptional CO_2 selectivity as a result of the rational inclusion of appropriately functionalized monomers; (iii) thermal stability due to strong covalent bond formation upon polymerization of the monomers; and (iv) structural diversity from the large library of monomers that can be used to construct the end product [15–18]. Such inherent chemical features make these materials ideal in pursuing in order to arrive at a solution for practical CO_2 capture [15].

Herein, we report on the design and synthesis of a novel microporous organic polymer, termed KFUPM-4, that was constructed from amine-functionalized and aromatic, polar heterocyclic monomers (aniline and pyrrole, respectively). KFUPM-4 was realized by an acid-catalyzed Friedel-Crafts polycondensation making use of *p*-formaldehyde as a

* Corresponding author.
E-mail address: othmanc@kfupm.edu.sa (O.C.S. Al Hamouz).

https://doi.org/10.1016/j.micromeso.2020.110391
Received 24 November 2019; Received in revised form 30 April 2020; Accepted 7 June 2020
Available online 23 June 2020
1387-1811/

crosslinking agent. The structure of this polymeric network was fully characterized and was demonstrated to have high surface area, CO_2 and H_2O thermodynamic (static) uptake capacities, and the ability to remove CO_2 from a CO_2/CH_4 natural gas stream in the presence of water without the loss of activity over several cycles.

2. Experimental section

2.1. Materials

Aniline (99% purity), pyrrole (98% purity), hydrochloric acid (37 wt %), thionyl chloride ($SOCl_2$; 97% purity), and dimethylsulfoxide (DMSO; ≥99.9% purity) were purchased from Millipore Sigma. *p*-Formaldehyde (≥9 9.9% purity) and anhydrous ferric chloride ($FeCl_3$; 97% purity) were purchased from Fluka. *N*,*N*′-Dimethylformamide (DMF, 99% purity) was obtained from Alpha Chemika. Methanol (MeOH; ≥ 99.9% purity) was acquired from Merck while ammonium hydroxide solution (NH_4OH; 28–30 *w/w*%) was obtained from Fisher Scientific. Prior to use, pyrrole was distilled at 150 °C under N_2 flow. Similarly, ferric chloride was dehydrated via reflux with thionyl chloride for 2 h, at which time thionyl chloride was distilled off and the freshly prepared dehydrated $FeCl_3$ was further dried under vacuum. All other chemicals were used without further purification. For gas adsorption measurements, ultrahigh purity grade nitrogen (99.999%), helium (99.999%), methane (99.9%) and high purity CO_2 (99.9%) were obtained from Abdullah Hashem Industrial Co., Dammam, Saudi Arabia.

2.2. Material characterization

Natural abundance solid-state ^{13}C nuclear magnetic resonance spectroscopy (NMR) measurements were performed on a Bruker 400 MHz spectrometer at ambient temperature operating at 125.65 MHz (11.74 T). In all measurement, the sample is packed into a 4 mm zirconia rotor, cross-polarization magic angle spinning (CP-MAS) and high-power decoupling were employed with a pulse delay of 5.0 s and a magic angle spinning rate of 10 kHz. Fourier-transform infrared spectra (FT-IR) was obtained on a PerkinElmer 16F PC FTIR spectrometer using solid potassium bromide (KBr) pellets. The spectra were recorded over a region of 4000–400 cm^{-1} (mid-IR region) in transmission mode. The output signals were described as follows: s, strong; m, medium; w, weak; and br, broad. Thermal gravimetric analysis (TGA) was performed on a QMS 403 C Aëolos with STA 449 F1 Jupiter instrument. The measurement was performed by heating up the sample to 1000 °C at a constant heating rate of 10 °C min^{-1} under air flow (99.99% purity). Differential scanning calorimetry (DSC) measurements were collected using a Netzsch-Gerätebau DSC 204 F1 Phoenix. In a typical experiment, the heating rate was set to 10 °C min^{-1} to reach a temperature of up to 500 °C. Low pressure gas adsorption measurements were performed using a Quantachrome Autosorb IQ instrument. Isotherms at 77 K were measured using a liquid nitrogen bath. For those isotherms measured at 273 and 298 K, a water circulator bath was used to ensure temperature stability. Water adsorption/desorption measurements were conducted on a Dynamic Vapor Sorption analyzer (DVS Vacuum, Surface Measurement Systems Ltd.). Prior to the measurement, the sample (~59 mg) was firstly pre-treated under vacuum at 110 °C for 12 h. The cycling measurement was then performed by water adsorption at 40 °C and desorption at 110 °C at 0.057 bar (76% RH). Powder X-ray diffraction (PXRD) measurements were recorded on a Rigaku MiniFlex II X-ray diffractometer with Cu Kα radiation (λ = 1.54178 Å).

2.3. Synthesis of KFUPM-4

Full synthetic and characterization details can be found in the Supplementary Information (SI), Section S1. To a 50 mL round-bottom flask equipped with a magnetic stirrer, *p*-formaldehyde (1.81 g, 0.06 mol) and anhydrous $FeCl_3$ (0.97 g, 0.006 mol) were added. The flask was then sealed and flushed with N_2 gas to create inert atmosphere. Aniline (1.1 mL, 0.92 g, 0.01 mol), pyrrole (2.0 mL, 2.01 g, 0.03 mol), and DMF (10 mL) were then injected into the sealed system. In a preheated oil bath, the reaction mixture was stirred at 80 °C for 24 h. After this time had elapsed, the reaction mixture was allowed to cool to room temperature, at which time, the solid was filtered via Buchner funnel, and the solid product was then washed with MeOH, ammonium hydroxide solution (to remove $FeCl_3$), distilled water, and, finally, with MeOH again. The product was then dried at 90 °C under vacuum until a constant weight was achieved. The final yield was 86% based on the weight of the product to the total sum of reactants.

2.4. Breakthrough measurements

Comprehensive details about the breakthrough set-up and the corresponding measurement parameters are provided in the SI, Section S3. In a typical measurement, a fixed bed was packed with KFUPM-4 powder and the sample was activated at 373 K for 24 h under vacuum prior to carrying out the measurement. The breakthrough experiments were conducted under ambient conditions (298 K and 1 bar) with a 10 sccm flowrate of CO_2:N_2 (20:80 *v/v*) and CO_2:CH_4 (10:90 *v/v*) feed mixtures. For the measurements under humid conditions, a dry N_2 or CH_4 gas stream was passed through a water humidifier at room temperature, which was then passed through the sample bed. The water level in the gas stream was monitored by mass spectrometry until saturation was obtained (91% RH). The full dynamic capacity of CO_2, N_2 and CH_4 were estimated by evaluating the ratio of compositions of the downstream gas and the feed gas. The regeneration of the sample was conducted at room temperature by flow of pure wet N_2 through the sample bed for 5–6 h.

3. Results and discussion

The design strategy for realizing an advanced functional polymeric material with intrinsic, permanent porosity and CO_2-philic properties focused on the judicious choice of building blocks. As such, the rigid aromatic and heterocyclic amines, aniline and pyrrole, were identified as suitable monomers. The decision to choose these units is an important one in that they both contain potentially accessible N atoms, which are well known to interact favorably with CO_2, and their molecular structures are rigid due to their aromaticity. In order to stitch together the respective building blocks to create a highly rigid, crosslinked network held together by strong covalent bonds, an acid-catalyzed Friedel-Crafts polycondensation synthetic strategy was adopted [13,16,17].

For the optimized reaction, aniline and pyrrole were dissolved in

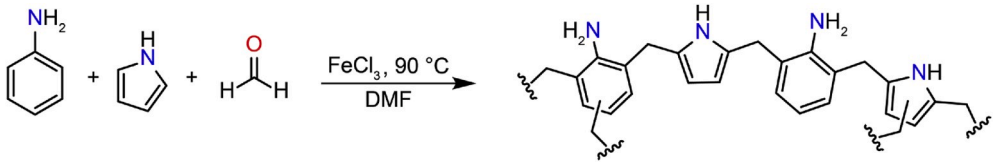

Scheme 1. KFUPM-4 was synthesized by an acid-catalyzed Friedel-Crafts polycondensation of aniline and pyrrole with *p*-formaldehyde acting as an external crosslinking agent. Due to the nature of the building blocks (aniline and pyrrole) as well as the external crosslinking agent (*p*-formaldehyde), the underlying structure of KFUPM-4 was demonstrated to be a highly crosslinked network held together by strong bonds.

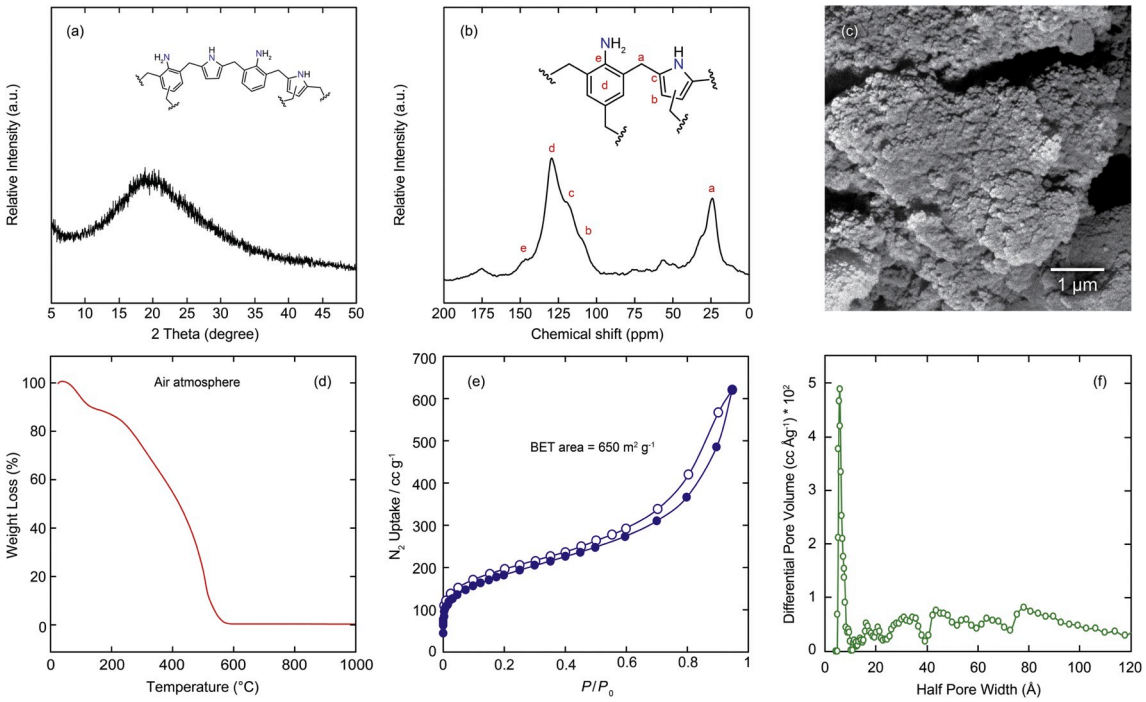

Fig. 1. Structural characterization of KFUPM-4. (a) Experimental PXRD pattern for KFUPM-4 showing the amorphous nature of the material. The core, underlying structure of the material is provided in the inset. (b) CP-MAS ^{13}C NMR spectrum at 10 KHz with the corresponding peak assignments provided. Inset: The core structure of the polymer is provided for peak assignment. (c) SEM image displaying the aggregating, submicrometer-sized particles. Scale bar: 1 μm. (d) TGA analysis under air flow demonstrating the thermal stability of KFUPM-4. (e) N_2 isotherm at 77 K. Filled and open circles correspond to the adsorption and desorption curves, respectively. (f) Pore size distribution of KFUPM-4 as calculated by quenched solid-state density functional theory model.

DMF in a molar ratio of 1:3, respectively, along with an excess amount of the external crosslinking agent, *p*-formaldehyde (SI, Section S1). The monomeric ratio was systematically varied during the optimization process and was ultimately decided upon after consistently producing a polymer with the highest intrinsic porosity. The acid catalyst source and quantity were also systematically varied. In the preliminary synthetic trials, two catalysts, hydrochloric acid and ferric chloride, were studied, from which it was determined that ferric chloride was significantly more active. By employing a high concentration of ferric chloride during the reaction, polymeric products were obtained with low surface areas and needing substantial post-synthetic treatment to remove residual catalyst. Consequentially, the synthetic trials revealed that 10 mol% of ferric chloride relative to *p*-formaldehyde was sufficient towards producing the end polymeric material with the requisite structural properties (SI, Section S1). With these optimized synthetic conditions in hand, the highly crosslinked, porous polymer product, KFUPM-4, was realized in 86% yield (Scheme 1). It is noted that prior to structural characterization, KFUPM-4 was thoroughly treated to remove any unreacted starting materials and/or ferric chloride catalyst.

To elucidate the underlying structure of KFUPM-4, from which both the presence and connectivity of the monomers can be confirmed, we employed a combination of powder X-ray diffraction (PXRD), Fourier transform infrared spectroscopy (FT-IR), cross-polarization magic angle spinning solid-state ^{13}C nuclear magnetic resonance spectroscopy (CP-MAS ^{13}C NMR), scanning electron microscopy (SEM), and thermal gravimetric analysis (TGA) techniques. As expected, KFUPM-4 was found to be X-ray amorphous by PXRD analysis and, therefore, lacked long-range periodicity (Fig. 1A) [18]. The presence of both aniline and pyrrole in the structure was then initially confirmed by FT-IR (SI, Fig. S1). In the FT-IR spectrum, a broad absorption band ranging from 3300 to 3500 cm^{-1} was assigned to two characteristic stretching bands: (i) primary amine ($–NH_2$) from aniline; and (ii) a secondary amine (–NH–) from pyrrole. The crosslinking methylene unit, formed after the Friedel-Crafts reaction, was proven by observing a –CH stretching absorption band centered at 2920 cm^{-1}. A medium-to-strong band, centered at 1630 cm^{-1}, was identified as a $–NH_2$ scissoring absorption attributable to aniline. Finally, $–NH_2$ (694 cm^{-1}) and –NH– (755 cm^{-1}) wagging absorption bands from aniline and pyrrole, respectively, were also observed [19]. Additional direct structural support was provided by CP-MAS ^{13}C NMR measurements (Fig. 1B). A characteristic resonance peak at $\delta = 25$ ppm was assigned to the chemical shift corresponding to an aliphatic methylene ($–CH_2–$) unit that crosslinks two aromatic C atoms from either of the monomers [20]. Additionally, four distinct resonance peaks in the range of $\delta = 105–150$ ppm were clearly observed and attributed to the aromatic carbons of aniline and pyrrole [21,22]. When taken together, the FT-IR and CP-MAS ^{13}C NMR provide clear evidence for not only the incorporation of both monomers within the structure, but also the formation of a highly crosslinked network.

The surface morphology of KFUPM-4 was then investigated by SEM analysis. Consistent throughout all samples measured, the SEM images displayed agglomerated, sphere-like particles with uniform submicrometer dimensions (Fig. 1C). KFUPM-4 was demonstrated to be thermally stable up to 250 °C. After this temperature, the polymer network decomposed via combustion at 600 °C (Fig. 1D). Differential scanning calorimetry (DSC) thermograms of KFUPM-4 exhibit no melting endotherms – a finding that coincides with the high thermal stability and rigid structure of KFUPM-4 (SI, Fig. S1). The presence of a large exothermic transition peak in the DSC thermogram is likely correlated to the interchain crosslinking as well as solid-solid conformational changes toward the most thermodynamically stable structure [23].

The porosity properties of KFUPM-4 were analyzed by N_2 adsorption isotherms at 77 K. As shown in Fig. 1E, KFUPM-4 exhibits a steep uptake a low relative pressure ($P/P_0 < 0.1$) indicating its microporous nature [24]. It is noted that the isotherm does not reach saturation with a sharp uptick in adsorption occurring at high relative pressure ($P/P_0 > 0.9$). This phenomenon is likely attributable to interparticle condensation of N_2 as a result of macropore formation between individual particles [25].

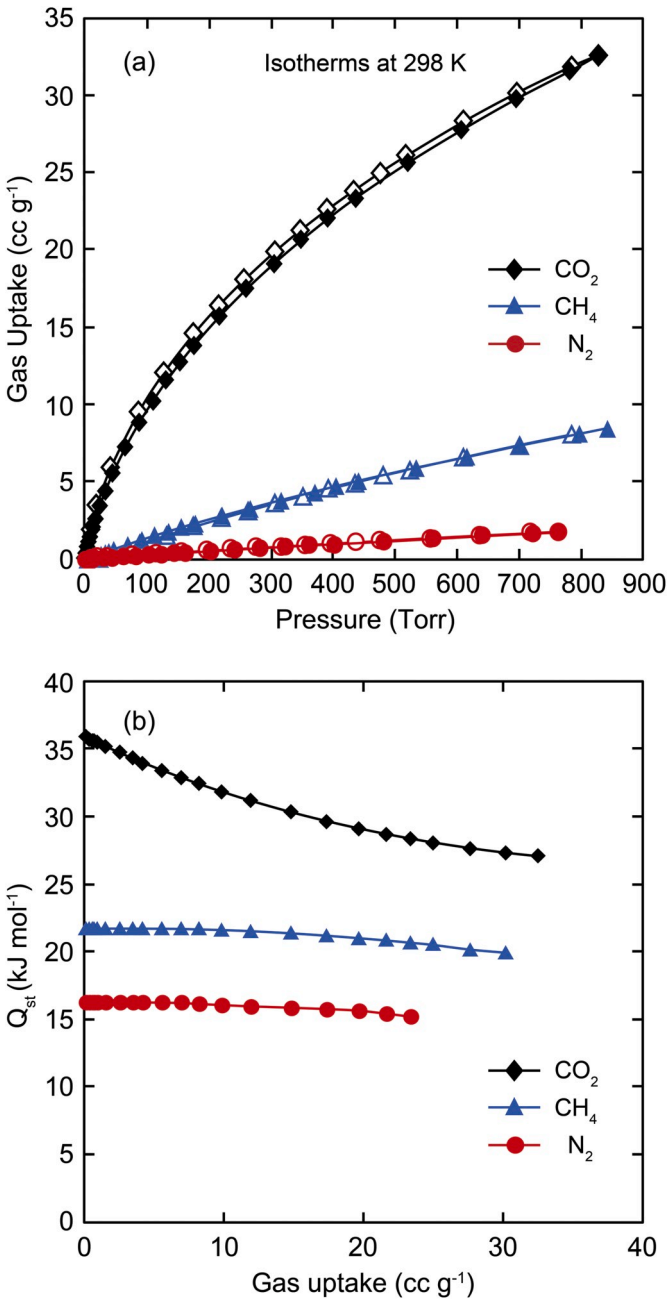

Fig. 2. (a) CO_2 (black diamonds), CH_4 (blue triangles), and N_2 (red circles) adsorption isotherms at 298 K for KFUPM-4. Filled and open symbols represent adsorption and desorption branches, respectively. The connecting lines are added as a guide for the eye. (b) Calculated enthalpy of adsorption (Q_{st}) of CO_2, CH_4, and N_2 for KFUPM-4. (For interpretation of the references to colour in this figure legend, the reader is referred to the Web version of this article.)

Indeed, as evidenced by SEM analysis, submicrometer KFUPM-4 particles are shown to aggregate thus providing the opportunity for interparticle macropore formation (Fig. 1C) [26]. Furthermore, a hysteretic behavior was observed upon desorption, which was attributed to elastic deformation or swelling of the crosslinked polymeric structure [27]. The Brunauer-Emmett-Teller (BET) surface area, calculated over the P/P_0 = 0.01–0.3 range, was 650 $m^2\ g^{-1}$. As a result of the interparticle condensation behavior, the total pore volume of KFUPM-4 (0.289 $cm^3\ g^{-1}$) was calculated using the Dubinin-Astakhov method. Finally, to provide further confirmation for the microporous nature of KFUPM-4, the pore size distribution (PSD) was also calculated using the quenched solid-state density functional theory (QSDFT) model. As such, the PSD of KFUPM-4 demonstrated that the pore sizes were found to be in both the microporous and mesoporous size region (Fig. 1F).

Given the high density of polar N atoms, the relatively small pore size, and the permanent porosity, we sought to assess KFUPM-4's performance towards capturing environmentally-harmful gases, such as CO_2 [3,28]. Accordingly, thermodynamic adsorption isotherms for CO_2 were measured at 298 and 273 K. As shown in Fig. 2A, the adsorption isotherm was fully reversible with only a slight appearance of hysteresis during desorption – a behavior that arises when a strong affinity is present. KFUPM-4 adsorbed 33 $cm^3\ g^{-1}$ (1.5 mmol g^{-1}) of CO_2 at 760 Torr and 298 K. Under these conditions, the CO_2 uptake capacity of KFUPM-4 is higher than similar porous organic adsorbents, such as KFUPM-2 (23.5 $cm^3\ g^{-1}$) [22], AZO-COP-1 (32 23.4 $cm^3\ g^{-1}$) [29] and CMP-1 (29.6 $cm^3\ g^{-1}$) [30] and comparable with others such as LZU-301 (COF) (35.6 $cm^3\ g^{-1}$) [31] and CTF-DCN-500 (38.4 $cm^3\ g^{-1}$) [32]. To assess the material's sorption capacities toward other gases that may be found in gas streams containing CO_2, we measured thermodynamic adsorption isotherms for CH_4 and N_2 at 298 and 273 K (Fig. 2A). As expected, KFUPM-4 adsorbs considerably less CH_4 (8.5 $cm^3\ g^{-1}$; 0.38 mmol g^{-1}) and N_2 (1.8 $cm^3\ g^{-1}$; 0.08 mmol g^{-1}) than CO_2 at 298 K and 760 Torr.

To assess the ability of an adsorbent material to selectively capture a specific gas molecule from a mixed gas stream, one must also consider how strongly the material interacts with each component of the gas stream. A useful qualitative approach for understanding the interactions of a gas molecule with an adsorbent material is to analyze the initial slopes of the isotherms [33]. As is evident in Fig. 2A, the initial slope for CO_2 adsorption is considerably steeper than the slopes observed for CH_4 and N_2 – an observation that points to the likelihood that KFUPM-4 interacts more strongly to CO_2 than to CH_4 and N_2. This qualitative assessment was then supported by the quantitative determination of the isosteric heat of adsorption (Q_{st}). Accordingly, a virial-type expansion equation was used to fit the CO_2, CH_4, and N_2 isotherms at 298 and 273 K (SI, Section S2). The resultant initial Q_{st} value for CO_2 was calculated to be 36 kJ mol^{-1} in comparison to 22 and 16 kJ mol^{-1} for CH_4 and N_2, respectively (Fig. 2B). The significantly larger Q_{st} value for CO_2 is indicative of KFUPM-4's stronger binding affinity to CO_2 when compared to CH_4 and N_2. It is noted that this Q_{st} value for CO_2 is comparable to similarly related adsorbents: BILP-1 (26.5 kJ mol-1) [34] Azo-COP-1 (29.3 kJ mol-1) [29]. With these results, the CO_2/N_2 and CO_2/CH_4 selectivities were then calculated using Henry's law. KFUPM-4 demonstrated exceptional CO_2/N_2 and CO_2/CH_4 selectivities of 79 and 15, respectively at 298 K. Indeed, these values are among the highest reported for porous organic materials [35]. Finally, to establish the material's long-term stability towards CO_2 adsorption, we measured 18 consecutive CO_2 adsorption-desorption cycles at 298 K (SI, Section S2). The results revealed a negligible loss in activity over the cycles, thus, providing support of KFUPM-4's long-term adsorption capabilities.

A primary concern for solid adsorbents in the practical removal of CO_2 from any mixed gas stream (*e.g.* flue gas, biogas, natural gas, among others) is the presence of water due to its competitive adsorption properties [7,11]. To investigate the interaction between water and KFUPM-4, vapor adsorption cycling measurements (21 cycles total; >120 h) were performed at 76% relative humidity and 40 °C (SI, Section S2). KFUPM-4 exhibited excellent stability towards water as evidenced by an uptake capacity of 12.8 wt% (Cycle 1) and 12.0 wt% (Cycle 20). The ability of KFUPM-4 to ad- and desorb water over a long period of time lends credence to the prospect that this material is viable for the dehydration of natural gas through reduction of the impact of water corrosion as well as the formation of hydrates [36,37].

Given the considerably high thermodynamic CO_2 uptake capacity, isosteric heat of adsorption, and selectivity over N_2 and CH_4 together with KFUPM-4's high water stability, we sought to demonstrate the material's ability to selectively separate CO_2 from mixed gas streams under dynamic conditions (*i.e.* breakthrough measurements). Accordingly, a fixed bed of KFUPM-4 was subjected to a dry gaseous mixture

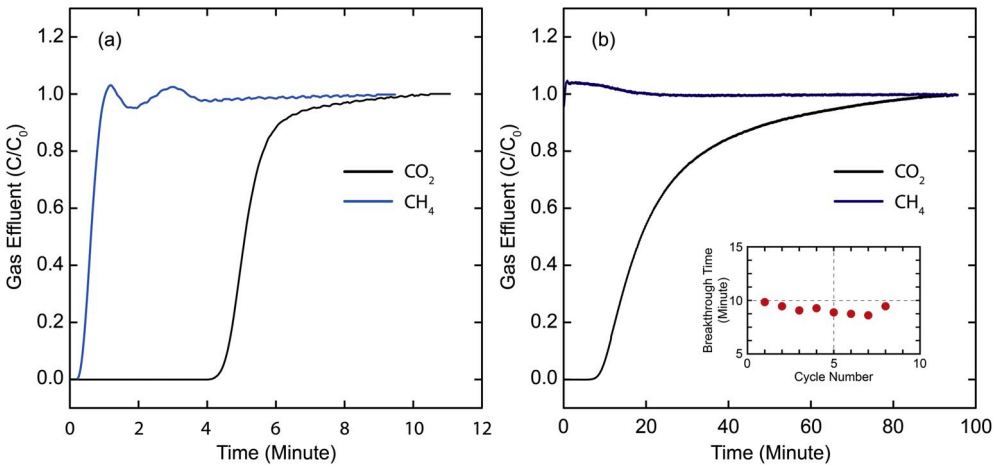

Fig. 3. (a) CO_2/CH_4 (10/90% *v/v*, respectively) breakthrough measurement at 298 K under dry conditions. (b) CO_2/CH_4 (10/90% *v/v*, respectively) breakthrough measurement at 298 K under wet conditions (91% relative humidity). The breakthrough curve shown is for the ninth consecutive cycle. Inset: Variation of breakthrough time as a function of breakthrough cycle number.

comprised of 10% CO_2 and 90% CH_4 (*v/v*) at 298 K – a ratio that mirrors that found in natural gas streams. As shown in Fig. 3A, the experimental breakthrough curves clearly exhibit CH_4 passing directly through the fixed bed of KFUPM-4 while CO_2 is retained for ~4.5 min. From this measurement, the dynamic CO_2 uptake capacity of KFUPM-4 was calculated to be 6.7 $cm^3\ g^{-1}$. Though this result is exciting in its own right, the competitive water adsorption problem remains to be tested. As such, the same breakthrough measurement was performed (10% CO_2 and 90% CH_4 (*v/v*) at 298 K) albeit with the introduction of water vapor to the gas stream as well (91% RH) (Fig. 3B). Surprisingly, the experimental breakthrough curve displayed an enhanced CO_2 breakthrough time (~9 min) resulting in a significant increase in dynamic CO_2 uptake capacity (13.8 $cm^3\ g^{-1}$). It is noted that the CH_4 breakthrough time and dynamic uptake capacity remained relatively unchanged. The enhancement in dynamic CO_2 uptake capacity in the presence of water is attributed to an enhanced solubility of CO_2 with better access to the amine functionalities within the micropores of KFUPM-4 [38]. This 'wet' breakthrough measurement was then repeated over 9 consecutive cycles with no significant loss of selectivity nor capacity. It is noted that between each cycle KFUPM-4 was regenerated by a simple N_2 flow at room temperature (Fig. 3B inset). This regeneration protocol is attractive in that it is energy-efficient, which represents a marked advantage over existing technologies employed [39].

4. Conclusions

In conclusion, we have reported the design, synthesis, and characterization of a novel highly rigid, crosslinked porous polymer, termed KFUPM-4. The synthesis of KFUPM-4 was optimized by changing the monomer ratio, reaction conditions (solvent, temperature, reaction time) and catalyst. The optimized porous polymer showed permanent porosity with a BET surface area of 650 $m^2\ g^{-1}$. As a result of its porosity and polarizable internal surface area, KFUPM-4 achieved a high CO_2 uptake capacity (33 $cm^3\ g^{-1}$ at 760 Torr and 298 K) and a high selectivity towards CO_2 over N_2 (79) and CH_4 (15) – both of which are among the highest selectivity values for these gas pairs among similarly related polymer materials. To demonstrate its practical applicability, KFUPM-4 was stable, with no loss of activity, toward the adsorption of CO_2 and H_2O over multiple cycles. The dynamic capacity measured from the breakthrough experiments revealed an increase in the adsorption capacity of CO_2 from 6.7 $cm^3\ g^{-1}$ under dry conditions (CO_2:CH_4 = 10:90% *v/v*, respectively; 298 K) and 13.8 $cm^3\ g^{-1}$ under wet conditions (CO_2:CH_4 = 10:90% *v/v*, respectively; 298 K; 91% RH) with a negligible loss in capacity over multiple cycles. The breakthrough and adsorption measurements reveal the exceptional features of KFUPM-4 and its potential use for the purification of natural gas.

Declaration of competing interest

The authors declare that they have no known competing financial interests or personal relationships that could have appeared to influence the work reported in this paper.

CRediT authorship contribution statement

Ahmed M. Alloush: Data curation, Investigation. **Mahmoud M. Abdelnaby:** Data curation, Investigation. **Kyle E. Cordova:** Formal analysis, Writing - review & editing. **Naef A.A. Qasem:** Data curation, Investigation. **Bassem A. Al-Maythalony:** Formal analysis. **Almaz Jalilov:** Formal analysis. **Youcef Mankour:** Formal analysis. **Othman Charles S. Al Hamouz:** Project administration, Resources, Supervision, Funding acquisition, Investigation, Methodology, Writing - original draft, Conceptualization.

Acknowledgments

We are grateful to Prof. Rached Ben-Mansour (KACST-TIC on CCS, KFUPM) for the use of his breakthrough instrument. Financial support for this project was provided by Saudi Aramco (Project No. 6510895769).

Appendix B. Supplementary data

Supplementary data to this article can be found online at https://doi.org/10.1016/j.micromeso.2020.110391.

All authors contributed to this manuscript equally under the supervision of Prof. Othman Al Hamouz.

References

[1] J.H. Mercer, West Antarctic ice sheet and CO_2 greenhouse effect: a threat of disaster, Nature 271 (1978) 321–325.
[2] R. York, Do alternative energy sources displace fossil fuels? Nat. Clim. Change 2 (2012) 441–443.
[3] L. Zou, Y. Sun, S. Che, X. Yang, X. Wang, M. Bosch, Q. Wang, H. Li, M. Smith, S. Yuan, Z. Perri, H.C. Zhou, Porous organic polymers for post-combustion carbon capture, Adv. Mater. 29 (2017), 1700229.
[4] C.A. Trickett, A. Helal, B.A. Al-Maythalony, Z.H. Yamani, K.E. Cordova, O. M. Yaghi, The chemistry of metal–organic frameworks for CO_2 capture, regeneration and conversion, Nat. Rev. Mater. 2 (2017), 17045.

[5] H.A. Patel, S. Hyun Je, J. Park, D.P. Chen, Y. Jung, C.T. Yavuz, A. Coskun, Unprecedented high-temperature CO2 selectivity in N_2-phobic nanoporous covalent organic polymers, Nat. Commun. 4 (2013) 1357.

[6] L. Liu, D. Nicholson, S.K. Bhatia, Impact of H_2O on CO_2 separation from natural gas: comparison of carbon nanotubes and disordered carbon, J. Phys. Chem. C 119 (2015) 407–419.

[7] R. Babarao, J. Jiang, Upgrade of natural gas in rho zeolite-like metal-organic framework and effect of water: a computational study, Energy Environ. Sci. 2 (2009) 1088–1093.

[8] J. Yu, Y. Ma, P.B. Balbuena, Evaluation of the impact of H_2O, O_2, and SO_2 on postcombustion CO_2 capture in metal-organic frameworks, Langmuir 28 (2012) 8064–8071.

[9] L. Ohlin, P. Bazin, F. Thibault-Starzyk, J. Hedlund, M. Grahn, Adsorption of CO_2, CH_4, and H_2O in zeolite ZSM-5 studied using in situ ATR-FTIR spectroscopy, J. Phys. Chem. C 117 (2013) 16972–16982.

[10] S. Li, G. Alvarado, R.D. Noble, J.L. Falconer, Effects of impurities on CO_2/CH_4 separations through SAPO-34 membranes, J. Membr. Sci. 251 (2005) 59–66.

[11] P. Billemont, B. Coasne, G. De Weireld, An experimental and molecular simulation study of the adsorption of carbon dioxide and methane in nanoporous carbons in the presence of water, Langmuir 27 (2011) 1015–1024.

[12] Y. Sun, Q. Xue, Y. Zhou, L. Zhou, Sorption equilibria of CO_2/CH_4 mixture on activated carbon in presence of water, J. Colloid Interface Sci. 322 (2008) 22–26.

[13] S. Xu, Y. Luo, B. Tan, Recent development of hypercrosslinked microporous organic polymers, Macromol. Rapid Commun. 34 (2013) 471–484.

[14] J. Schmidt, D.S. Kundu, S. Blechert, A. Thomas, Tuning porosity and activity of microporous polymer network organocatalysts by co-polymerisation, Chem. Commun. 50 (2014) 3347–3349.

[15] D.M. D'Alessandro, B. Smit, J.R. Long, Carbon dioxide capture: prospects for new materials, Angew. Chem. 49 (2010) 6058–6082.

[16] L.B. Sun, Y.H. Kang, Y.Q. Shi, Y. Jiang, X.Q. Liu, Highly selective capture of the greenhouse gas CO_2 in polymers, ACS Sustain. Chem. Eng. 3 (2015) 3077–3085.

[17] M. Saleh, H.M. Lee, K.C. Kemp, K.S. Kim, Highly stable CO_2/N_2 and CO_2/CH_4 selectivity in hyper-cross-linked heterocyclic porous polymers, ACS Appl. Mater. Interfaces 6 (2014) 7325–7333.

[18] M. Errahali, G. Gatti, L. Tei, G. Paul, G.A. Rolla, L. Canti, A. Fraccarollo, M. Cossi, A. Comotti, P. Sozzani, L. Marchese, Microporous hyper-cross-linked aromatic polymers designed for methane and carbon dioxide adsorption, J. Phys. Chem. C 118 (2014) 28699–28710.

[19] M. Trchová, J. Stejskal, Polyaniline: the infrared spectroscopy of conducting polymer nanotubes (IUPAC technical report), Pure Appl. Chem. 83 (2011) 1803–1817.

[20] R. Dawson, T. Ratvijitvech, M. Corker, A. Laybourn, Y.Z. Khimyak, A.I. Cooper, D. J. Adams, Microporous copolymers for increased gas selectivity, Polym. Chem. 3 (2012) 2034–2038.

[21] X.G. Li, Y. Kang, M.R. Huang, Optimization of polymerization conditions of furan with aniline for variable conducting polymers, J. Comb. Chem. 8 (2006) 670–678.

[22] M.M. Abdelnaby, N.A.A. Qasem, B.A. Al-Maythalony, K.E. Cordova, O.C.S. Al Hamouz, A microporous organic copolymer for selective CO_2 capture under humid conditions, ACS Sustain. Chem. Eng. 7 (2019) 13941–13948.

[23] E.E.M. Ahmad, A.S. Luyt, V. Djoković, Thermal and dynamic mechanical properties of bio-based poly(furfuryl alcohol)/sisal whiskers nanocomposites, Polym. Bull. 70 (2013) 1265–1276.

[24] M. Thommes, K. Kaneko, A.V. Neimark, J.P. Olivier, F. Rodriguez-Reinoso, J. Rouquerol, K.S.W. Sing, Physisorption of gases, with special reference to the evaluation of surface area and pore size distribution (IUPAC technical report), Pure Appl. Chem. 87 (2015) 1051–1069.

[25] A.B. Soliman, R.R. Haikal, Y.S. Hassan, M.H. Alkordi, The potential of a graphene-supported porous-organic polymer (POP) for CO_2 electrocatalytic reduction, Chem. Commun. 52 (2016) 12032–12035.

[26] S. Wu, Y. Liu, G. Yu, J. Guan, C. Pan, Y. Du, X. Xiong, Z. Wang, Facile preparation of dibenzoheterocycle-functional nanoporous polymeric networks with high gas uptake capacities, Macromolecules 47 (2014) 2875–2882.

[27] J. Weber, M. Antonietti, A. Thomas, Microporous networks of high-performance polymers: elastic deformations and gas sorption properties, Macromolecules 41 (2008) 2880–2885.

[28] A.R. Millward, O.M. Yaghi, Metal-organic frameworks with exceptionally high capacity for storage of carbon dioxide at room temperature, J. Am. Chem. Soc. 127 (2005) 17998–17999.

[29] H.A. Patel, S.H. Je, J. Park, Y. Jung, A. Coskun, C.T. Yavuz, Directing the structural features of N_2 -phobic nanoporous covalent organic polymers for CO_2 capture and separation, Chem. Eur J. 20 (2014) 772–780.

[30] R. Dawson, L.A. Stevens, T.C. Drage, C.E. Snape, M.W. Smith, D.J. Adams, A. I. Cooper, Impact of water coadsorption for carbon dioxide capture in microporous polymer sorbents, J. Am. Chem. Soc. 134 (2012) 10741–10744.

[31] Y.X. Ma, Z.J. Li, L. Wei, S.Y. Ding, Y.B. Zhang, W. Wang, A dynamic three-dimensional covalent organic framework, J. Am. Chem. Soc. 139 (2017) 4995–4998.

[32] K. Wang, H. Huang, D. Liu, C. Wang, J. Li, C. Zhong, Covalent triazine-based frameworks with ultramicropores and high nitrogen contents for highly selective CO_2 capture, Environ. Sci. Technol. 50 (2016) 4869–4876.

[33] Y.S. Bae, R.Q. Snurr, Development and evaluation of porous materials for carbon dioxide separation and capture, Angew. Chem. 50 (2011) 11586–11596.

[34] M.G. Rabbani, H.M. El-Kaderi, Template-free synthesis of a highly porous benzimidazole-linked polymer for CO_2 capture and H_2 storage, Chem. Mater. 23 (2011) 1650–1653.

[35] H. Zhao, X. Luo, H. Zhang, N. Sun, W. Wei, Y. Sun, Carbon-based adsorbents for post-combustion capture: a review, Greenhouse Gas Sci. Technol. 8 (2018) 11–36.

[36] X. Lv, B. Shi, S. Zhou, H. Peng, Y. Lei, P. Yu, Study on the growth rate of natural gas hydrate in water-in-oil emulsion system using a high-pressure flow loop, RSC Adv. 8 (2018) 36484–36492.

[37] W. Zhao, T. Zhang, Y. Wang, J. Qiao, Z. Wang, Corrosion failure mechanism of associated gas transmission pipeline, Materials 11 (2018) 1935.

[38] J. Yu, Y. Zhai, S.S.C. Chuang, Water enhancement in CO_2 capture by amines: an insight into CO_2-H_2O interactions on amine films and sorbents, Ind. Eng. Chem. Res. 57 (2018) 4052–4062.

[39] G.T. Rochelle, Amine scrubbing for CO_2 capture, Science 325 (2009) 1652–1654.